Supplement Material

Materials and Methods

Animals The subcommittee on research for animal care at the Massachusetts General Hospital approved the experimental protocol. CC10-IL-6 transgenic mice (Tg(+)) were bred on a C57/BL6 (Tg(-)) background.[1] In these mice, the Clara cell 10-kD promoter (CC10) was used to constitutively drive lung-specific expression of IL-6. Tg(-) littermates served as controls in all experiments. Five Tg(-) and five Tg(+) mice, age- and sex-matched, were exposed to room air (21% FiO_2) and then another five Tg(-) and five Tg(+) mice age- and sex-matched, were exposed to hypoxia (10% FiO_2) at sea level. All animals were 3 months old and weighed 22.5 ± 2.0 grams.

For hypoxia, animals were placed in a sealed chamber. The O_2 concentration in the chamber was maintained at 10% by controlling the inflow rate of compressed air and N_2. Gas was circulated in the chamber with a fan. The CO_2 concentration was maintained at < 0.4% with a CO_2 absorbent. Gas samples were tested twice per day during the entire experimental period to monitor O_2 and CO_2 tension. The chamber was unsealed for less than 30 minutes twice per week to replenish the food, replace CO_2 absorbent and clean the cages.

Measurement of right ventricular systolic pressure (RVSP) All mice were administered ketamine (80 mg/kg) and diazepam (5 mg/kg), which produced anesthesia with spontaneous breathing. A midline sternal skin incision was made from the second intercostal space to the xiphoid process. A 25-gauge needle was attached to a male/male

luer slip connector, which was joined, in a successive order, to an 18-gauge blunt needle, polyethylene 190 tubing (ID 1.19 mm; OD 1.70 mm), 18-gauge blunt needle connected to a physiological transducer (Becton Dickinson DTXPlusDT-XX) via a two-way plastic stopcock. The stopcock facilitated flushing of the needle and *in situ* measurement of atmospheric pressure without introducing air bubbles. The entire system was flushed with sterile saline to eliminate bubbles. The transducer was positioned 1.0 cm above the level of the midaxillary line. The needle was then inserted into the right ventricle by following a 45º trajectory between the right second and third intercostal space above the xiphoid process. Pressures were recorded on a Gould chart recorder (Model RS3400) with an embedded Gould transducer amplifier (Model 13-4615-50) at paper speeds ranging from 2.5 to 200 mm/s. Peak RVSPs were obtained, as previously described.[2] Placement of the needle into the right ventricle was confirmed by postmortem examination.

Heart weight The right ventricular free wall was detached and removed under a dissecting microscope. The left ventricle and septum were weighed separately from the right ventricle, with measurements being taken after drying at 90ºC for 24 h and 48 h. If the difference between the two readings was greater than ± 0.5 mg, the specimens were dried for another 24 h.[2]

Histology of pulmonary vasculature and heart The heart and lungs were flushed with normal saline, removed and fixed in formalin for 72 h. The aorta was removed under a dissecting microscope to access the pulmonary trunk. Two 3-cm silicone tubes (0.03 cm

× 0.05 cm; SMI, Saginaw, MI) were inserted into the pulmonary trunk through a small opening that was made in the lateral wall to maintain vessel wall patency during fixation. One tube was advanced through the main artery into the right pulmonary artery while another tube was inserted into the left pulmonary artery until resistance was encountered at their respective hila. Both main branches of the PA were lifted away from the heart and lungs, using the tubing as an aid. The tubing was removed before tissue embedding. Both the formalin-inflated left lung and the whole heart were sliced into 5 μm-thick sections. Slices of the lung, heart, main pulmonary branches, and pulmonary trunk were dehydrated and embedded in paraffin. Sections were then stained with hematoxylin & eosin, elastic, and giemsa stains.

Assessment of pulmonary remodeling Pulmonary remodeling was assessed by the percent wall thickness of the main PA branches (central) and parenchymal PA vessels indexed to terminal bronchioles and acini (i.e., vessels indexed to respiratory bronchioles or alveolar ducts).[3] Wall thickness was measured with an ocular micrometer and expressed as the medial wall thickness (the distance between the internal and external lamina) divided by the diameter of the vessel (the distance between the external lamina) × 100 (% wall thickness; %WT). For vessels with a single elastic lamina, the distance between the elastica and endothelial basement membrane was measured.[2] The total number of peripheral arteries was expressed as the number of arteries per every 100 alveoli in each field and was verified using sections in which the vessels were stained with elastin.[4] A quantitative analysis of luminal obstruction was performed by counting at least 50 small pulmonary arterioles (outer diameter < 50 μm) in every hematoxylin-

eosin stained lung section. These arterioles were assessed for occlusive lesions and scored as follows: (1) no evidence of lumen occlusion (open), (2) partial (< 50%) luminal occlusion, and (3) full luminal occlusion (closed).[5] All morphometric analyses were performed by one blinded observer.

Antibodies Antibodies used for immunohistochemistry included rat anti-mouse B220 antigen (1:100; Clone RA3-6B2, BD Biosciences, San Diego, CA), rabbit polyclonal anti-human CD3 (1:400), polyclonal antibody to factor VIII-related antigen (1:250, Dakocytomation, Carpinteria, CA), and biotinylated goat anti-rabbit IgG (1:200; Vector laboratories, Inc., Burlingame, CA). Mouse monoclonal FLK-1 (VEGF-R2, Clone A3, Santa Cruz Biotechnology, Inc., Santa Cruz, CA) was used at a dilution of 1:200 for immunoblot and 1:50 for immunohistochemistry. Anti-actin smooth muscle specific (AB-2) mouse mAb(1A4) (1:750; EMD Chemicals, Inc., Gibbstown, NJ). Antibodies used for immunoblot include mouse monoclonal VEGF antibody (1:1000; Abcam, Cambridge, MA), TGF-β antibody (rabbit polyclonal antibody; 1:1000), TNF-α (rabbit polyclonal antibody; 1:200), goat anti-rabbit IgG -HRP(1:2000), p38 (rabbit monoclonal antibody total 1:500 and phosphorylated 1:200), JNK (rabbit polyclonal antibody total 1:500 and phosphorylated JNK 1:50), c-MYC (rabbit polyclonal antibody 1:200), β-actin (rabbit polyclonal antibody, 1:2000), caspase 3 (rabbit polyclonal antibody 1:200), cleaved caspase 3 (rabbit monoclonal antibody 1:200), survivin (rabbit polyclonal antibody 1:400), Bcl-2 (rabbit polyclonal antibody 1:200) and BAX (rabbit polyclonal antibody 1:400) from Cell Signaling Technology, Inc; Danvers, MA), PDGF-B (rabbit polyclonal antibody 1:100), MCP-1 (rabbit polyclonal antibody 1:100), ERK1/2 (rabbit

polyclonal, 1:500; Clone 14), and MAX (rabbit polyclonal antibody; 1:50) from Santa Cruz Biotechnology, Inc., Santa Cruz, CA. Goat anti-mouse IgG (1:2000; Jackson Immunoresearch Laboratories, Philadelphia, PA), anti-fractalkine (0.1 μg/ml; cleaved c-CX_3CL1 [30 kDa] and total CX_3CL1, R & D Systems, Inc., Minneapolis, MN).[6] Purified mouse anti-NF-ATc3 monoclonal antibody (1:200; BD Biosciences, Franklin Lakes, NJ).

Immunohistochemistry Formalin-fixed, paraffin-embedded tissue sections were baked for 10 min at 60ºC, deparaffinized, and rehydrated. For antigen retrieval, tissues were rinsed in water and heated in a Decloaker pressure cooker in 0.01M Na-citrate (pH 6.0) for 3 min. The Na-citrate bath was returned to room temperature (RT) before the sections were rinsed in water. Endogenous peroxidase activity was quenched by treating sections with 3% H_2O_2 for 5 min. Sections were then washed in phosphate-buffered saline (PBS) and successively blocked for 15 min at RT with appropriate serum, avidin, and biotin. Tissue sections were incubated with primary antibodies overnight at 4ºC, washed with PBS, and if necessary (if primary was not biotinylated), incubated with secondary biotinylated antibody for 1 h at RT. Bound antibodies were detected by treating sections with streptavidin-horseradish peroxidase complex for 30 min. Peroxidase activity was visualized with 3,3' diaminobenzidine, and sections were counterstained with hematoxylin. Primary antibody was omitted from staining reactions as a negative control. Thymus and spleen tissue served as positive controls for leukocyte staining.

Immunoblotting Frozen lung tissue was homogenized for 30 min on ice in RIPA buffer (50 mM Tris-HCl [pH 7.4], 150 mM NaCl, 1% NP-40, 0.5% sodium deoxycholate, 0.1%

SDS; Boston BioProducts, Worcester, MA) supplemented with phosphatase inhibitor (Calbiochem, La Jolla, CA) and protease inhibitor (Calbiochem). Homogenates were centrifuged at 2000 rpm at 4ºC for 30 min, and centrifugation was repeated on the supernatants. The protein concentration of the resulting supernatant was determined using Bradford reagent (Bio-Rad Laboratories, Hercules, CA). Proteins (70 μg) were electrophoresed on 4 – 20% gradient Tris-Hepes-SDS gels (Pierce, Rockford IL) and transferred to Immobilon PVDF membranes (Millipore Corporation, Bedford, MA). Prestained molecular mass marker proteins (Bio-Rad Laboratories) were used as standards for the Tris-Hepes-SDS gel electrophoresis. The PVDF membranes were blocked with 5% non-fat dry milk in Tris-Buffered Saline containing 0.1% tween-20 (TBST) for 1 h at RT, washed with TBST, and probed with primary antibody diluted in blocking buffer for 2 h at RT. The membrane was subsequently washed, incubated with secondary antibody diluted in blocking buffer for 1 h at RT. Antibody labeling was visualized using chemiluminescence reagent (Cell Signaling Technology).

TdT-mediated dUTP nick end labeling staining. End labeling of exposed 3'-OH ends of DNA fragments was undertaken with the TdT-mediated dUTP nick end labeling (TUNEL) in situ cell death detection kit (FragEL, Calbiochem, La Jolla, CA).

Statistical analysis. Data are expressed as mean ± s.e.m. Multiple comparisons were made using the non-parametric Kruskal-Wallis test, and statistical significance ($p \leq 0.05$) between two groups was confirmed using the non-parametric Wilcoxon-Mann-Whitney test. Statistics were performed using Statview 4.5 (Abacus Concepts, Inc., Berkeley,

CA). In all experiments, n is equal to 5 replicates apart from immunoblots where the n is equal to 4 replicates.

Results

IL-6 overexpression increases pulmonary artery pressure and ventricular hypertrophy (expanded)

To test the hypothesis that increased IL-6 may cause increased PVR and PAH, we measured the right ventricular systolic pressure (RVSP) by direct right ventricular puncture, in transgenic mice over expressing IL-6 (Tg(+)). Under normoxic conditions, Tg(+) mice had elevated RVSP compared to Tg(-) mice (34 ± 2 mmHg vs. 21 ± 1 mmHg, $p<0.05$, Figure 1a). In Tg(+) mice, 3 weeks of exposure to 10% oxygen almost doubled RVSP to 64 ± 7 mmHg ($p<0.05$ vs. normoxic), and this value was almost 2.6 times higher than the RVSP in hypoxic Tg(-) mice (24 ± 1 mmHg, $p<0.05$, Figure 1a). As in C57B1/6 mice,[7] Tg(-) mice did not exhibit any significant increase in RVSP in response to hypoxia (compared to normoxic controls).

Ventricular wall thickness increased in response to chronic pressure overload, which is a consequence of elevated resistance in the pulmonary artery (PA). Right ventricular hypertrophy (RVH), as measured by right ventricle weight / (left ventricle weight + septum weight; RV/LV+S) and absolute right ventricle weight (RV), were greater in Tg(+) mice than in Tg(-) mice under normoxic conditions (RV/LV+S: 0.4 ± 0.02 vs. 0.3 ± 0.02, $p<0.05$, Figure 1b and RV: 0.007 ± 0.0001 gm vs. 0.005 ± 0.00001 gm, $p<0.05$, Figure1 b, c). Hypoxia produced even greater RVH in Tg(+) mice (RV/LV+S: 0.7 ± 0.1, and RV: 0.01 ± 0.001 gm, $p<0.05$ vs. normoxic control) while there was no change in ventricular wall thickness in Tg(-) mice (Figure 1c). The absolute

left ventricle weight remained unchanged between groups (data not shown). The histological appearance of the hearts was consistent with RVH measurements, showing that, in both normoxic and hypoxic conditions, right ventricular wall mass was greater in Tg(+) mice (Figure 1d).

IL-6 overexpression induced muscularization throughout the entire pulmonary vascular bed (expanded)

To determine the cause of increased PVR, we examined specific regions of the pulmonary vascular tree for remodeling. Examination of the proximal branches of the main PA revealed that the elastic lamina was increased in normoxic Tg(+) mice compared to their Tg(-) counterparts (Figure 2 c vs. a) and was quantitatively confirmed by counting the number of elastic lamina (3 ± 0.3 vs. 2 ± 0.0, $p<0.05$; Figure 2q). Following hypoxia, the number of elastic lamina in Tg(+) mice was increased to 10 ± 1(figure 2d), which exceeded the number in normoxic Tg(+) mice ($p<0.05$) and hypoxic Tg(-) littermates (2 ± 0.3, $p<0.05$; Figure 2q). No differences in the number of elastic lamina between normoxic and hypoxic Tg(-) mice were observed. Main PA branches in Tg(+) mice exhibited an increase in not only the number of elastic lamina, but also the percent vessel medial wall thickness, relative to the Tg(-) control, under both normoxic ($7 \pm 1\%$ vs. $3 \pm 1\%$, $p<0.05$) and hypoxic conditions ($15 \pm 1\%$ vs. $6 \pm 1\%$, $p<0.05$; Figure 2r). The medial wall of the main PA branches in Tg(+) mice more than doubled in thickness in response to hypoxia compared to their Tg(+) normoxic controls ($15\pm 1\%$ vs. $7 \pm 1\%$, $p<0.05$), while PA medial wall thickness did not change in hypoxic Tg(-) mice compared to normoxic controls.

The terminal bronchioles (TB) and distal acinar arterioles were examined for evidence of muscularization. The most notable findings were that the distal acinar arterioles of Tg(+) mice were muscularized at baseline and became more thickly muscularized in hypoxia unlike the Tg(-) mice arterioles as shown by elastic staining (Figure 2 Tg(+) k, l vs. Tg(-) i, j) and by immunohistochemistry with α-smooth muscle actin (Figure 2 Tg(+) o, p vs. Tg(-) m, n).

Quantitatively, we found that TB medial wall thickness was greater in normoxic Tg(+) mice than normoxic Tg(-) mice (29 ± 2% vs. 24 ± 2%, $p<0.05$, Figure 2s). The same was true of the acinar medial walls (26 ± 1% vs. 21 ± 1%, $p<0.05$, Figure 2t). Under hypoxic conditions, medial wall thickness for Tg(+) mice was greater than that for Tg(-) mice in both the TBs (49 ± 4% vs. 30 ± 3%, $p<0.05$, Figure 2s) and acini (49 ± 1% vs. 32 ± 2%, $p<0.05$, Figure 2t). In Tg(+) mice, hypoxia nearly doubled medial wall thickness for both the TB vessels (49 ± 4% vs. 29 ± 2% for normoxic control, $p<0.05$, Figure 2s) and acinar vessels (49 ± 1% vs. 26 ± 1% for normoxic control, $p<0.05$, Figure 2t). In Tg(-) mice, hypoxia induced only a 1 – 1.5-fold change in medial wall thickness for TB vessels (30 ± 3% vs. 24 ± 2% for normoxic control, $p<0.05$) and acinar vessels (32 ± 2% vs. 21 ± 1% for normoxic control, $p<0.05$).

Hypoxia induced loss of pulmonary arterioles in IL-6 overexpressing mice.

To test whether a reduction in arterioles may contribute to the increase PVR in Tg(+) mice, we compared the number of arterioles (per every 100 alveoli) in the alveolar bed of Tg(+) and Tg(-) mice. Vessel number did not significantly differ between these mice under normoxic conditions. Hypoxia reduced the number of countable arterioles at the alveolar level in both Tg(+) mice (7 ± 1 vs. 12 ± 1 for normoxic control, $p<0.05$) and

Tg(-) mice (11 ± 1 vs. 14 ± 1 for normoxic control, p = 0.05), and the relative arteriolar reduction was similar for both groups (Online Figure I). However, Tg(+) mice had a lower number of arterioles compared to their Tg(-) littermates (7 ± 1 vs. 11 ± 1, $p<0.05$). Therefore, the hypoxia-induced reduction in the number of distal pulmonary vessels is similar for Tg(+) and Tg(-) mice, but the absolute reduction is greater in Tg(+) mice.

Characterization of Pulmonary Vasculopathy in IL-6 Tg (+) Mice: Growth Factors.

To determine the factors that stimulate growth of PAEC and PASMC, immunoblot analysis of whole lung lysates (Online Figure IIa) was performed. We first confirmed that both VEGF and VEGFR2 levels were higher in Tg(+) mice than Tg(-) mice under normoxic conditions and hypoxic conditions. Transforming growth factor (TGF)-β, a pro-apoptotic anti-proliferative protein, was reduced in Tg(+) mice compared to Tg(-) mice under normoxic conditions and hypoxic conditions, while platelet derived growth factor (PDGF) was similarly increased in all groups. This suggests that IL-6 is promoting cellular growth by up-regulating growth factor VEGF and preventing inhibition of cellular growth by down-regulating TGF-β.

Characterization of Pulmonary Vasculopathy in IL-6 Tg(+) Mice: Mitogen Activated Protein Kinases.

We evaluated for evidence of signal transduction pathways that may be linking pro-growth factor responses to intracellular downstream pro-proliferative transcription factors. We found that phosphorylated extracellular regulated kinase (ERK), a pro-proliferative growth mitogen activated protein kinase (MAPK), was elevated in Tg(+)

lung lysates compared to Tg(-) lysates in both normoxic and hypoxic conditions (Online Figure IIb). Pro-apoptotic MAPKinases such as p38 and pJNK were not increased in Tg(+) lung lysates compared to Tg(-) lysates in both normoxic and hypoxic conditions. Taken together this would suggest that IL-6 is specifically activating pro-proliferative growth kinase ERK while preventing the activation of kinases that promote apoptosis.

Characterization of Pulmonary Vasculopathy in IL-6 Tg(+) Mice: Pro-Proliferative and Anti-Apoptotic Targets.

Given that cellular proliferation is increased within the walls of the pulmonary vasculature of the IL-6 Tg(+) mice (Figure 4 k, l, and o) and proliferative MAPK ERK is increased (Online Figure IIb), we evaluated for evidence of downstream proliferative transcription factors. We found that c-myc, a basic-helix-loop-helix/leucine zipper transcription factor that controls the G1-S cell cycle promoting cellular growth and proliferation,[8] was elevated in Tg(+) mice relative to their Tg(-) counterparts under normoxic and hypoxic conditions (Online Figure IIc). In addition, c-Myc's obligate binding partner, MAX, was also exclusively elevated in Tg(+) mice relative to their Tg(-) counterparts under normoxic and hypoxic conditions. This suggests that IL-6 may be inducing cellular growth and proliferation and subsequent pulmonary vascular wall remodeling by up-regulating pro-proliferative oncogenic transcription proteins.

Given that the growth inhibitor TGF-β, and two MAPKinases that stimulate downstream apoptotic signals, phosphorylated 38 and JNK, are reduced, we investigated if

downstream pro-apoptotic caspase 3 is modulated by IL-6 in these mice. Cleaved caspase 3 activity was increased in IL-6 Tg(+) mice at baseline compared to Tg(-) mice. However in hypoxia cleaved caspase 3 activity was reduced in Tg(+) mice compared with baseline room air conditions (Online Figure IId). In order to determine if programmed cell death is occurring in the distal arteriolar lesions, we looked for DNA fragmentation, a marker of apoptosis, and observed that in the IL-6 Tg(+) mice, there was DNA fragmentation in epithelial cells and possibly in histiocytes of alveolar units but not in the walls of the distal arterioles (Online Figure IIe). Taken together, IL-6 overexpression may be selectively preventing programmed cell death by apoptosis within the pulmonary vascular bed.

To determine which anti-apoptotic proteins may be involved in inhibiting caspase 3 and preventing subsequent cell death within the vascular bed, we probed for two important anti-apoptotic proteins, Bcl-2 and survivin. We found that Bcl-2 was elevated in Tg(+) mice relative to their Tg(-) counterparts under normoxic and hypoxic conditions (Online Figure IId) while pro-apoptotic protein BAX levels were similar in Tg(-) and Tg(+) mice and remained unchanged in hypoxic conditions. We found that survivin is markedly elevated in Tg(+) mice compared to Tg(-) mice at baseline and in hypoxia (Online Figure IId). This suggests that IL-6 may be inducing a pro-survival cellular state by modulating several anti-apoptotic proteins.

Characterization of Lymphocyte Recruitment and Function.

To determine the signals that IL-6 employs to control the recruitment of lymphocytes, we probed for chemokines that are known to be involved in lymphocyte trafficking. We found that Tg (+) mice had elevated levels of activated fractalkine (c-CX_3CL1), a PAEC-derived chemokine that recruits T cells and mediates T cell adhesion to endothelial cells, at baseline and in hypoxic conditions (Online Figure III). Monocyte chemoattractant protein, MCP-1, a chemokine that recruits monocytes and lymphocytes and may have a role in smooth muscle cell proliferation was increased in IL-6 Tg (+) mice at room air but was reduced in hypoxia (Online Figure III). Tumor necrosis factor (TNF)-alpha was reduced in both normoxic and hypoxic conditions in the IL-6 Tg (+) mice compared to Tg (-) mice. Nuclear factor of activated T-cells, cytoplasmic, calcineurin-3 (NF-ATc3), which may have a role in promoting a state of proliferation and suppress mitochondrial–dependent apoptosis[9], was slightly increased in IL-6 Tg (+) mice whole lung lysates (Online Figure III). Taken together, this data supports the concept that overexpression of IL-6 stimulates the recruitment of T cells through up-regulation of specific chemokines depending on the presence or absence of hypoxia and stimulates T cells to home to distal pulmonary arteriole vessels. In turn, T cells may be enhancing IL-6's pro-survival apoptotic resistant cellular phenotypic effects.

Discussion

IL-6 and cMyc/MAX Expanded

IL-6 overexpression may predispose to exaggerated PAH as a result of coordinating a number of downstream pro-proliferative, pro-survival, and anti-apoptotic signaling pathways (Figure 6). We found that c-myc, and its obligate binding partner, MAX may

be key in IL-6's downstream proliferative signal cascade, promoting cellular proliferative phenotypes in PAH. Consistent with our findings, endothelin stimulated rat aortic smooth muscle cells are shifted into a pro-proliferative state in the presence of ERK induced c-myc activation.[10] It also has been shown that pulmonary arteries from rats exposed to hypoxia have elevated levels of c-myc mRNA.[11] In addition, YY1 growth regulator of vascular smooth muscle cells targets c-myc downstream leading to increased smooth muscle specific gene expression, proliferation and neonatal piglet pulmonary hypertension.[12] Furthermore, in the presence of TGF-β/BMP proteins, c-myc expression is attenuated contributing to PASMC apoptosis.[13] How the c-myc/max complex may be altering its target cell cycle genes and whether the additional stress of hypoxia may alter its effects on downstream targets is unclear at present. However, given the number of angioproliferative lesions at baseline, which likely results in localized hypoxia, and the increase in the number of lesions in hypoxia, we hypothesize, based on extensive work in tumor hypoxia deprivation biology,[8] that hypoxia inducible factors may be facilitating the formation of c-myc-max complex and thereby augmenting the expression of cell cycle genes and exaggerating the hyper-proliferative cellular phenotypes in this transgene mouse. Further investigation with this IL-6 Tg(+) mouse will allow us to evaluate the role of IL-6 in the presence of hypoxia and associated physiologic changes thus imposed by hypoxic vasoconstriction.

IL-6 and Apoptosis Expanded

While IL-6 appears to be driving a number of proteins that promote cellular proliferation, it is also clear from our work that IL-6 is also affecting apoptosis by down regulating

TGF-β and pro-apoptotic MAPKs, pJNK and p38 (Figure 6). As with hyperoxic injury in Tg(+) mice[14] and H_2O_2 injury in IL-6 stimulated endothelial cells,[15] caspase 3, the main gate keeper to programmed cell death, appears to be activated at baseline and is subsequently down-regulated when under the stress of hypoxia. However, evidence for DNA fragmentation, a marker of apoptosis, is observed only in epithelial cells and possibly histiocytes lining the alveoli, not in the cells of the obliterative lesions of the distal pulmonary vasculature at baseline or in hypoxia. This would suggest that IL-6's role in preventing cell death by apoptosis is PA wall specific at baseline and persists in hypoxia. Dysregulation of mediators of apoptosis in the PA wall of patients with PAH favoring suppression of apoptosis has been shown in gene microarray studies.[16] Anti-apoptotic proteins Bcl-2 and survivin have been found to be up-regulated in patients with PAH[16, 17] where they are thought to impair the activity of Kv channels[17, 18]and subsequent mitochondria-dependent apoptosis.[19] Similar to patients with PAH, IL-6 Tg(+) mice also share a similar anti-apoptotic biology with increased expression of both bcl-2 and survivin. At present, it remains unclear what triggers induced by IL-6 modulate the expression of these two anti-apoptotic proteins. However it is clear that DNA fragmentation within the complex obliterative vascular lesions of L-6 Tg(+) mice is absent favoring a pro-proliferative cell state, as observed in angioproliferative lesions of patients with PAH.

IL-6 and Inflammation Expanded

Elevation of IL-6 in PAH patients suggests that cellular immunity may play an active role in the dysregulation of PAEC and PASMC and the development of PAH. Accordingly,

plexigenic and concentric lesions in patients with severe PAH contain inflammatory cells, consisting of T cells, macrophages, and to a lesser extent, B cells[20, 21]. Similarly, the obliterative complex distal arterial lesions in Tg(+) mice also contain an abundance of T cells and to a lesser extent, B cells, while B cells appear to surround the large and mid sized airways.[22] The mechanisms underlying inflammatory cell recruitment and transendothelial migration into pulmonary artery vessel walls during PAH are unclear, although the chemokines RANTES[23] and fractalkine[24] may participate in inflammatory cell trafficking.[25] Hyper-proliferative PAEC may mediate the adhesion of the T lymphocytes by over-expressing fractalkine, as the cleaved activated form of fractalkine is up-regulated in the lungs of IL-6 Tg(+) mice as well as in plexigenic lesions of patients.[24] Further work examining T lymphocyte trafficking in Tg(+) mice will be instrumental in understanding their role in the vascular changes seen in patients with PAH.

There has been much controversy regarding the role of T cells in PAH, where T cell-mediated immunity has been found to be protective against PAH in VEGFR blocker treated nude rats[5] while in antigen challenged mice the Th2 immune response is associated with vascular muscularization.[26] In the IL-6 Tg(+) mouse, IL-6 and T cells may have a trans-signaling relationship, whereby T cell activation driven by IL-6 contributes to the perpetuation of IL-6's pro-inflammatory pro-proliferative anti-apoptotic effects on neighboring PASM and PAEC (Figure 6). Such a relationship has been thought to have been an important mechanism underlying other chronic inflammatory diseases,[27] and may be one of the many important IL-6 mechanisms involved in the pathogenesis of PAH. NFAT proteins, produced and carried to PA

vessels in lymphocytes have recently been noted to be activated in human PAH and may be contributing to the resistance to apoptosis within the PA wall. In IL-6 Tg(+) mice, NF-ATc3 was only slightly increased in the IL-6 Tg(+) mice compared with Tg(-) mice at baseline and in hypoxia, and therefore may or may not be associated with PAEC and PASMC insensitivity to apoptosis. Its significance may be under-represented by the lack of cell specificity as it was tested in whole lung lysates. Taken together, T cells in an IL-6 rich milieu are prominently situated within the distal arteriolar vessels, and further work to evaluate their role, whether protective or stimulatory, will be key to understanding their presence in human PAH disease.

IL-6 and Loss of PA vessels Expanded

Whether the loss of small pulmonary arteriolar vessels contributes to the development of PVR is controversial. The importance of this loss may be negligible since chronic hypoxic experimental PAH models have considerable angiogenesis[28] and Rho kinase inhibitors normalize pulmonary pressures during chronic hypoxia via vasodilation.[29] However, vessel loss is induced by many other experimental PAH stimuli, including injection of monocrotaline,[30] monocrotaline combined with pneumonectomy,[31, 32] chronic hyperoxia,[32] and creation of aortopulmonary shunts.[33] Clinically, artery loss occurs in idiopathic PAH,[34] as well as in conditions associated with PAH, including congenital heart disease[35] and lung developmental abnormalities.[36] Here, hypoxia induced a significant loss of distal arterioles in Tg(+) mice, which are known to have abnormal alveoli with enlarged terminal air sacs.[1] This altered anatomy, which may result in a significant decrease in the number of arterioles, could significantly contribute to

increased PVR. We found no significant differences in vessel number between Tg(-) and (+) mice under normoxic conditions and the hypoxia-induced arteriolar reduction was similar between groups, despite a significant increase in PVR in Tg(+) hypoxic mice. Thus, arterial vessel loss alone may not account for increased PVR in IL-6 Tg(+) mice.

References:

1. Ward NS, Waxman AB, Homer RJ, Mantell LL, Einarsson O, Du Y, Elias JA. Interleukin-6-Induced Protection in Hyperoxic Acute Lung Injury. *Am J Respir Cell Mol Biol.* 2000;22:535-542.

2. Zhu YJ, Kradin R, Brandstetter RD, Staton G, Moss J, Hales CA. Hypoxic pulmonary hypertension in the mast cell-deficient mouse. *Journal of Applied Physiology: Respiratory, Environmental & Exercise Physiology.* 1983;54:680-686.

3. Quinn DA, Du HK, Thompson BT, Hales CA. Amiloride analogs inhibit chronic hypoxic pulmonary hypertension. *American Journal of Respiratory & Critical Care Medicine.* 1998;157:1263-1268.

4. Merklinger SL, Wagner RA, Spiekerkoetter E, Hinek A, Knutsen RH, Kabir MG, Desai K, Hacker S, Wang L, Cann GM, Ambartsumian NS, Lukanidin E, Bernstein D, Husain M, Mecham RP, Starcher B, Yanagisawa H, Rabinovitch M. Increased fibulin-5 and elastin in S100A4/Mts1 mice with pulmonary hypertension. *Circulation Research.* 2005;97:596-604.

5. Taraseviciene-Stewart L, Nicolls MR, Kraskauskas D, Scerbavicius R, Burns N, Cool C, Wood K, Parr JE, Boackle SA, Voelkel NF. Absence of T cells confers increased pulmonary arterial hypertension and vascular remodeling. *American Journal of Respiratory & Critical Care Medicine.* 2007;175:1280-1289.

6. Habasque C, Satie AP, Aubry F, Jegou B, Samson M. Expression of fractalkine in the rat testis: molecular cloning of a novel alternative transcript of its gene that is differentially regulated by pro-inflammatory cytokines. *Mol Hum Reprod.* 2003;9:449-455.

7. Raoul W, Wagner-Ballon O, Saber G, Hulin A, Marcos E, Giraudier S, Vainchenker W, Adnot S, Eddahibi S, Maitre B. Effects of bone marrow-derived cells on monocrotaline- and hypoxia-induced pulmonary hypertension in mice. *Respir Res.* 2007;8:8.

8. Huang LE. Carrot and stick: HIF-alpha engages c-Myc in hypoxic adaptation. *Cell Death Differ.* 2008;15:672-677.

9. Bonnet S, Rochefort G, Sutendra G, Archer SL, Haromy A, Webster L, Hashimoto K, Bonnet SN, Michelakis ED. The nuclear factor of activated T cells in pulmonary arterial hypertension can be therapeutically targeted. *Proc Natl Acad Sci U S A.* 2007;104:11418-11423.

10. Chen S, Qiong Y, Gardner DG. A role for p38 mitogen-activated protein kinase and c-myc in endothelin-dependent rat aortic smooth muscle cell proliferation. *Hypertension.* 2006;47:252-258.

11. Cai Y, Han M, Luo L, Song W, Zhou X. Increased expression of PDGF and c-myc genes in lungs and pulmonary arteries of pulmonary hypertensive rats induced by hypoxia. *Chin Med Sci J.* 1996;11:152-156.

12. Favot L, Hall SM, Haworth SG, Kemp PR. Cytoplasmic YY1 is associated with increased smooth muscle-specific gene expression: implications for neonatal pulmonary hypertension. *Am J Pathol.* 2005;167:1497-1509.

13. Fantozzi I, Platoshyn O, Wong AH, Zhang S, Remillard CV, Furtado MR, Petrauskene OV, Yuan JX. Bone morphogenetic protein-2 upregulates expression and function of voltage-gated K+ channels in human pulmonary artery smooth muscle cells. *Am J Physiol Lung Cell Mol Physiol.* 2006;291:L993-1004.

14. Ward NS, Waxman AB, Homer RJ, Mantell LL, Einarsson O, Du Y, Elias JA. Interleukin-6-induced protection in hyperoxic acute lung injury. *American Journal of Respiratory Cell & Molecular Biology.* 2000;22:535-542.

15. Waxman AB, Mahboubi K, Knickelbein RG, Mantell LL, Manzo N, Pober JS, Elias JA. Interleukin-11 and Interleukin-6 Protect Cultured Human Endothelial Cells from H2O2-Induced Cell Death. *Am J Respir Cell Mol Biol.* 2003;29:513-522.

16. Geraci MW, Moore M, Gesell T, Yeager ME, Alger L, Golpon H, Gao B, Loyd JE, Tuder RM, Voelkel NF. Gene expression patterns in the lungs of patients with primary pulmonary hypertension: a gene microarray analysis. *Circulation Research.* 2001;88:555-562.

17. McMurtry MS, Archer SL, Altieri DC, Bonnet S, Haromy A, Harry G, Bonnet S, Puttagunta L, Michelakis ED. Gene therapy targeting survivin selectively induces

pulmonary vascular apoptosis and reverses pulmonary arterial hypertension.[see comment]. *Journal of Clinical Investigation.* 2005;115:1479-1491.

18. Ekhterae D, Platoshyn O, Krick S, Yu Y, McDaniel SS, Yuan JX. Bcl-2 decreases voltage-gated K+ channel activity and enhances survival in vascular smooth muscle cells. *Am J Physiol Cell Physiol.* 2001;281:C157-165.

19. Altieri DC. Validating survivin as a cancer therapeutic target. *Nat Rev Cancer.* 2003;3:46-54.

20. Tuder RM, Groves B, Badesch DB, Voelkel NF. Exuberant endothelial cell growth and elements of inflammation are present in plexiform lesions of pulmonary hypertension.[see comment]. *Am J Pathol.* 1994;144:275-285.

21. Cool CD, Kennedy D, Voelkel NF, Tuder RM. Pathogenesis and evolution of plexiform lesions in pulmonary hypertension associated with scleroderma and human immunodeficiency virus infection. *Human pathology.* 1997;28:434-442.

22. DiCosmo BF, Geba GP, Picarella D, Elias JA, Rankin JA, Stripp BR, Whitsett JA, Flavell RA. Airway epithelial cell expression of interleukin-6 in transgenic mice. Uncoupling of airway inflammation and bronchial hyperreactivity. *Journal of Clinical Investigation.* 1994;94:2028-2035.

23. Dorfmuller P, Zarka V, Durand-Gasselin I, Monti G, Balabanian K, Garcia G, Capron F, Coulomb-Lhermine A, Marfaing-Koka A, Simonneau G, Emilie D, Humbert M. Chemokine RANTES in severe pulmonary arterial hypertension. *American Journal of Respiratory & Critical Care Medicine.* 2002;165:534-539.

24. Balabanian K, Foussat A, Dorfmuller P, Durand-Gasselin I, Capel F, Bouchet-Delbos L, Portier A, Marfaing-Koka A, Krzysiek R, Rimaniol AC, Simonneau G,

Emilie D, Humbert M. CX(3)C chemokine fractalkine in pulmonary arterial hypertension.[see comment]. *American Journal of Respiratory & Critical Care Medicine.* 2002;165:1419-1425.

25. Springer TA. Traffic signals for lymphocyte recirculation and leukocyte emigration: the multistep paradigm. *Cell.* 1994;76:301-314.

26. Daley E, Emson C, Guignabert C, de Waal Malefyt R, Louten J, Kurup V, Hogaboam C, Taraseviciene-Stewart L, Voelkel N, Rabinovitch M, Grunig E, Grunig G. Pulmonary arterial remodeling induced by a Th2 immune response. *The Journal of Experimental Medicine.* 2008;205:361-372.

27. Atreya R, Mudter J, Finotto S, Mullberg J, Jostock T, Wirtz S, Schutz M, Bartsch B, Holtmann M, Becker C, Strand D, Czaja J, Schlaak JF, Lehr HA, Autschbach F, Schurmann G, Nishimoto N, Yoshizaki K, Ito H, Kishimoto T, Galle PR, Rose-John S, Neurath MF. Blockade of interleukin 6 trans signaling suppresses T-cell resistance against apoptosis in chronic intestinal inflammation: evidence in crohn disease and experimental colitis in vivo. *Nat Med.* 2000;6:583-588.

28. Howell K, Preston RJ, McLoughlin P. Chronic hypoxia causes angiogenesis in addition to remodelling in the adult rat pulmonary circulation. *J Physiol (Lond).* 2003;547:133-145.

29. Hyvelin JM, Howell K, Nichol A, Costello CM, Preston RJ, McLoughlin P. Inhibition of Rho-kinase attenuates hypoxia-induced angiogenesis in the pulmonary circulation. *Circulation Research.* 2005;97:185-191.

30. Ye CL, Rabinovitch M. Inhibition of elastolysis by SC-37698 reduces development and progression of monocrotaline pulmonary hypertension. *American Journal of Physiology.* 1991;261:H1255-1267.

31. O'Blenes SB, Fischer S, McIntyre B, Keshavjee S, Rabinovitch M. Hemodynamic unloading leads to regression of pulmonary vascular disease in rats.[see comment]. *J Thorac Cardiovasc Surg.* 2001;121:279-289.

32. Koppel R, Han RN, Cox D, Tanswell AK, Rabinovitch M. Alpha 1-antitrypsin protects neonatal rats from pulmonary vascular and parenchymal effects of oxygen toxicity. *Pediatr Res.* 1994;36:763-770.

33. Rendas A, Lennox S, Reid L. Aorta-pulmonary shunts in growing pigs. Functional and structural assessment of the changes in the pulmonary circulation. *J Thorac Cardiovasc Surg.* 1979;77:109-118.

34. Meyrick B, Clarke SW, Symons C, Woodgate DJ, Reid L. Primary pulmonary hypertension: a case report including electronmicroscopic study. *Br J Dis Chest.* 1974;68:11-20.

35. Rabinovitch M, Keane JF, Norwood WI, Castaneda AR, Reid L. Vascular structure in lung tissue obtained at biopsy correlated with pulmonary hemodynamic findings after repair of congenital heart defects. *Circulation.* 1984;69:655-667.

36. Bohn D, Tamura M, Perrin D, Barker G, Rabinovitch M. Ventilatory predictors of pulmonary hypoplasia in congenital diaphragmatic hernia, confirmed by morphologic assessment. *J Pediatr.* 1987;111:423-431.

Legend (Supplement)

Online Figure I The number of arteries per 100 alveoli in IL-6 Tg(+) and Tg(-) mice in normoxic conditions are similar at baseline. Under hypoxic conditions, the number of arteries per 100 alveoli are reduced in both Tg(+) and Tg(-) mice (‡ vs. normoxic Tg(+);$p<0.05$, † vs. normoxic Tg(-);$p<0.05$) with IL-6 Tg(+) mice having the highest reduction (‡ vs. hypoxic Tg(-);$p<0.05$).

Online Figure II (**a**) Representative immunoblot protein expression of TGF-β, PDGF, VEGF, and VEGFR2 of lung lysates from IL-6 Tg(+) and Tg(-) mice exposed to normoxia and 3 weeks of hypoxia. (**b**) Representative immunoblot protein expression of phosphorylated ERK 42, ERK 42/44, phosphorylated p38, p38, phosphorylated JNK-1 and JNK2/3, and JNK.(**c**) Representative immunoblot protein expression of PCNA, c-myc, and MAX. (**d**) Representative immunoblot protein expression of survivin, Bcl-2, BAX, cleaved caspase-3, and caspase 3. β-actin used as control. (**e**) Representative photomicrographs of distal acinar arterioles of the PA vasculature of IL-6 Tg(+) and Tg(-) mice in normoxic and hypoxic conditions exposed to TdT-mediated dUTP nick end labeling (TUNEL) for DNA fragmentation evaluation. The distal arterioles (arrow with dark circle) and specifically the occlusive lesions in Tg(+) mice at baseline and in hypoxia have no evidence of DNA fragmentation, while epithelial cells and possibly histiocytes lining the alveolar walls are TUNEL positive at baseline (arrow, see inset). TUNEL staining, magnification x400, bar=0.001mm and inset, magnification x1000, bar=0.0005mm. β-actin used as a control.

Online Figure III Representative immunoblot protein expression of TNF-α, MCP-1, cleaved chemokine fractalkine (c-CX_3CL1), total CX_3CL1, NF-ATc3, T cells (CD3) and B cells (CD19) in whole lung lysates of IL-6 Tg (+) and Tg (-) mice exposed to normoxia and 3 weeks of hypoxia. β-actin used as a control.

Online Figure I

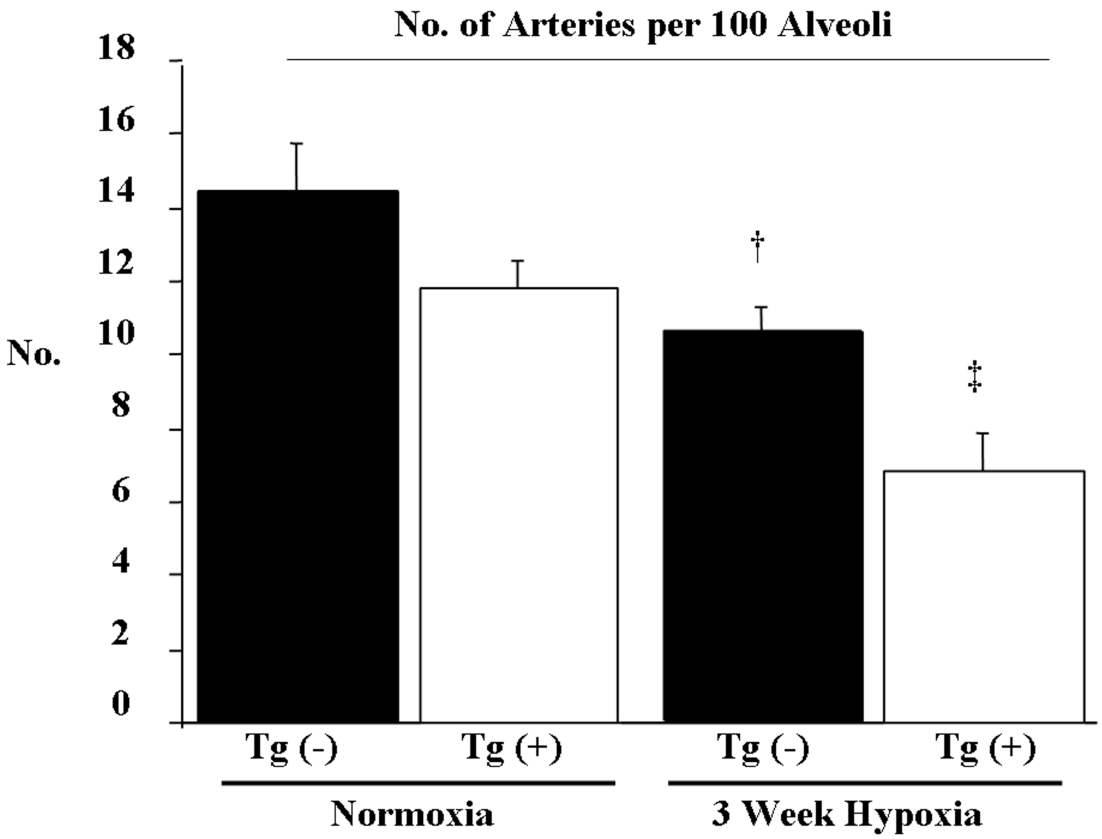

Online Figure II

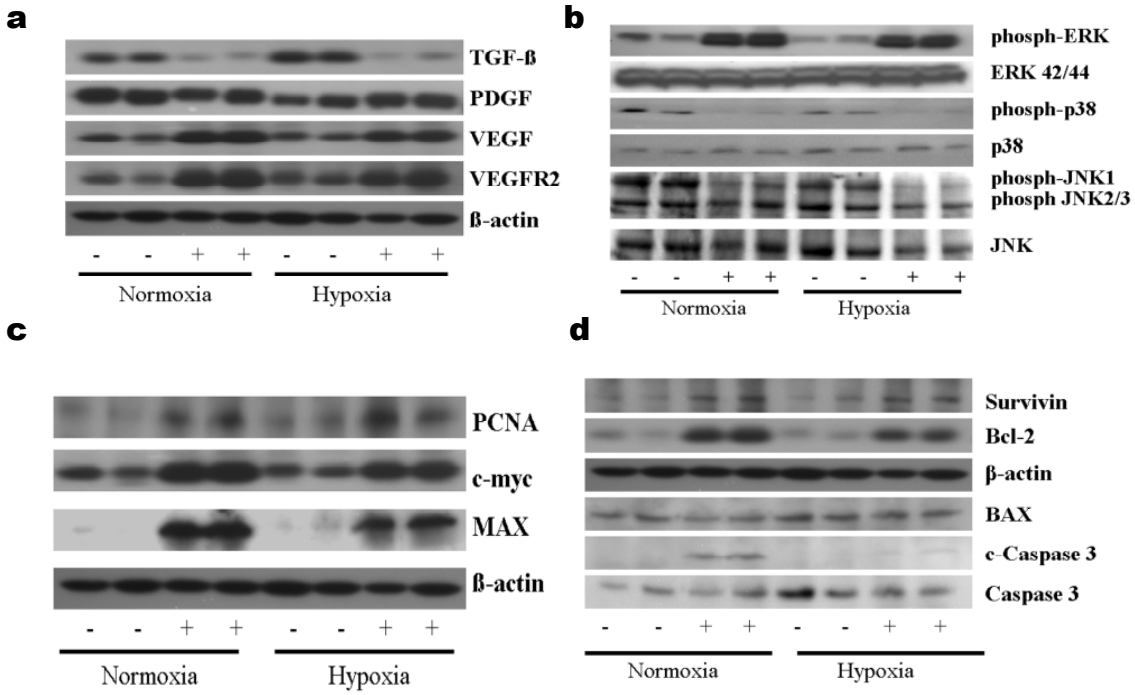

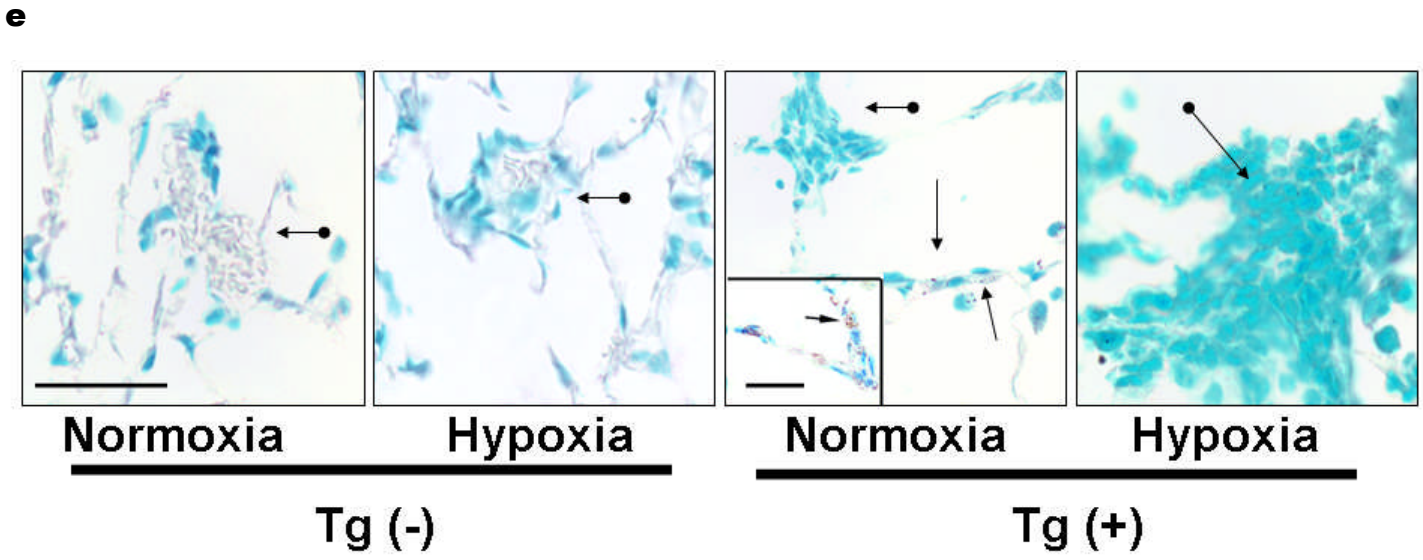

Online Figure III